Quantum interferences in the $\gamma N \to e^+e^-N$ reaction close to the vector meson production threshold

Matthias F. M. Lutz

GSI, Planckstrasse 1, D-64291 Darmstadt, Germany

Madeleine Soyeur

DAPNIA/SPhN, CEA/Saclay, F-91191 Gif-sur-Yvette Cedex, France

Abstract

The exclusive photoproduction of e^+e^- pairs from nucleons close to the vector meson production threshold ($1.4 < \sqrt{s} < 1.8$ GeV) results from two main processes: the emission of Bethe-Heitler pairs and the photoproduction of ρ^0- and ω-mesons decaying into e^+e^- pairs. The Bethe-Heitler amplitudes are purely electromagnetic and reflect mostly the nucleon magnetic structure. The $\gamma N \to e^+e^-N$ amplitudes arising from vector meson production and decay are derived from $\gamma N \to \rho^0 N$ and $\gamma N \to \omega N$ amplitudes supplemented by the Vector Meson Dominance assumption. The vector meson photoproduction amplitudes are calculated using a relativistic and unitary coupled-channel approach to meson-nucleon scattering. They depend sensitively on the coupling of vector fields to baryon resonances. The $\gamma N \to e^+e^-N$ differential cross sections display interference patterns. The interference of Bethe-Heitler pair production with vector meson e^+e^- decay is quite small in the domain of validity of our model for all angles of the emitted e^+e^- pair. The interference of ρ^0- and ω-mesons in the e^+e^- channel can be large. It is constructive for the $\gamma p \to e^+e^-p$ reaction and destructive for the $\gamma n \to e^+e^-n$ reaction. We discuss the shape and magnitude of the e^+e^- pair spectra produced in the $\gamma p \to e^+e^-p$ and $\gamma n \to e^+e^-n$ reactions as functions of the pair emission angle and of the total center of mass energy $\sqrt{s}$. In the particular kinematics under consideration, our results suggest that the vector meson contribution can be determined quite accurately from experimental e^+e^- spectra by subtracting the Bethe-Heitler term and neglecting the small interference of Bethe-Heitler pairs with vector meson e^+e^- decays.

Key words: Vector meson production; Baryon resonances; Dileptons; Quantum interference

PACS: 13.20; 13.60.Le; 14.20.Gk

1 Introduction

The scattering of real and virtual photons off nucleon targets is the simplest process to study the electromagnetic structure of the nucleon and its excitation to baryon resonances through vector fields. The link between vector fields and photons is established by assuming the Vector Meson Dominance (VMD) of the electromagnetic current [1,2]. We consider photon-nucleon kinematics such that the total center of mass energy is in the mass range of low-lying baryon resonances ($1.4 < \sqrt{s} < 1.8$ GeV).

Real Compton scattering, $\gamma N \to \gamma N$, appears mostly sensitive to the radiative widths (couplings) of baryon resonances and to the partial wave structure of single- and double-pion photoproduction processes [3]. Virtual Compton scattering, $e^- N \to e^- \gamma N$, offers the possibility to study photon-nucleon scattering amplitudes induced by virtual space-like photons, $\gamma^* N \to \gamma N$. The degree of virtuality of the incoming photon, which can be either longitudinal or transverse, provides an additional variable. The $e^- N \to e^- \gamma N$ cross section involves however more than the $\gamma^* N \to \gamma N$ amplitudes. The radiation of a photon from the incoming or outgoing electron contributes largely to the cross section and interferes with the $e^- N \to e^- \gamma N$ amplitudes arising from virtual photon-nucleon scattering. The $e^- p \to e^- \gamma p$ reaction in the resonance region has been measured recently [4]. In view of the s-channel baryon resonance contributions to this process, it is interesting that data on the $e^- p \to e^- \pi^0 p$ reaction were taken simultaneously, providing information on the coupling of the intermediate baryon resonances to the pion-nucleon channel [5]. The $\gamma\, N \to e^+ e^- N$ reaction makes it possible to explore yet another sector of photon-nucleon scattering, the photoproduction of virtual time-like photons, $\gamma N \to \gamma^* N$. In this case also there is an additional amplitude of electromagnetic origin: the initial photon can radiate an $e^+ e^-$ pair (Bethe-Heitler pair). These processes, the production of Bethe-Heitler pairs and the $e^+ e^-$ decay of time-like photons, will in general interfere. The contribution of the $\gamma N \to \gamma^* N$ transition amplitude to the $\gamma\, N \to e^+ e^- N$ reaction is of much interest. In the Vector Meson Dominance model of the electromagnetic current, it is indeed sensitive to the decay of low-lying baryon resonances into the vector meson nucleon channel below the ρ^0- and ω-meson threshold. The corresponding couplings are largely unknown and of importance to study models of baryon resonances [6] and vector meson propagation in matter [7]. The contributions of ρ^0- and ω-decays to the $\gamma\, N \to e^+ e^- N$ cross section will also display interference patterns. We consider $e^+ e^-$ pair invariant masses not too far from the vector meson poles where the Vector Meson Dominance assumption is expected to be valid and where significant constraints arise from the $\gamma\, N \to \rho^0 N$ and $\gamma\, N \to \omega N$ reactions. We note that, just as the $e^- N \to e^- \gamma N$ and $e^- N \to e^- \pi N$ processes give information on two decay channels of the baryon resonances excited in virtual photon-nucleon scattering, the $\gamma\, N \to e^+ e^- N$ and $\pi\, N \to e^+ e^- N$ reac-

tions select different entrance channels for the excitation of these resonances. Combined descriptions of both processes are therefore particularly invaluable to study the coupling of baryon resonances to specific decay channels. Extending such a comparison to higher invariant masses ($\sqrt{s} \simeq 2.1$ GeV) might be very relevant to study the issue of the 'missing resonances' predicted by constituent quark models and unobserved in the pion-nucleon channel [8].

In the spirit of the above discussion, we have studied the $\gamma N \to e^+e^-N$ reaction in the same theoretical framework as the $\pi N \to e^+e^-N$ reaction [9]. We use the $\gamma N \to \rho^0 N$ and $\gamma N \to \omega N$ amplitudes obtained in the unitary coupled-channel model of Ref. [7] to calculate the $\gamma N \to e^+e^-N$ amplitudes resulting from vector meson decays. We take the same prescription as in Ref. [9] for the Vector Meson Dominance of the electromagnetic current associated with the outgoing time-like photon.

There are at present no experimental data to compare our predicted cross sections to. Early attempts to measure the photoproduction of electron-positron pairs from proton targets at MAMI (Mainz), using tagged photons with energy ranging from 536 to 820 MeV, failed to obtain statistically significant results for e^+e^- pair invariant masses beyond 200 MeV [10,11]. Data on the photoproduction of e^+e^- pairs from deuterium and nuclear targets (carbon, iron, lead) were recently taken at JLab with the CLAS detector [12]. The laboratory photon energy varies from 0.9 until about 3 GeV. These data are in the process of being analyzed. As the $\gamma n \to e^+e^-n$ reaction has a much lower cross section than the $\gamma p \to e^+e^-p$ reaction, the $\gamma d \to e^+e^-X$ process should be dominated by $\gamma p \to e^+e^-p$ in specific regions of phase space (corresponding to the largest e^+e^- pair invariant masses) and hence provide a first test of our theoretical model.

We discuss the various amplitudes contributing to the $\gamma N \to e^+e^-N$ processes in Section 2. The calculation of the $\gamma p \to e^+e^-p$ and $\gamma n \to e^+e^-n$ cross sections is described in Section 3. Some intermediate steps of our derivations are explained in the appendix. Our numerical results on both reactions are displayed and commented upon in Section 4. We stress interference phenomena and show how they depend on the initial photon energy and on the emission angle and invariant mass of the e^+e^- pair. We conclude by a few remarks in Section 5.

2 The Bethe-Heitler and vector meson photoproduction amplitudes contributing to the $\gamma N \to e^+e^-N$ reactions

The $\gamma N \to e^+e^-N$ cross section is obtained by summing the amplitudes for the direct and crossed Bethe-Heitler terms and for the photoproduction of ρ^0- and ω-mesons decaying subsequently into e^+e^- pairs. This is represented graphically in Fig.1.

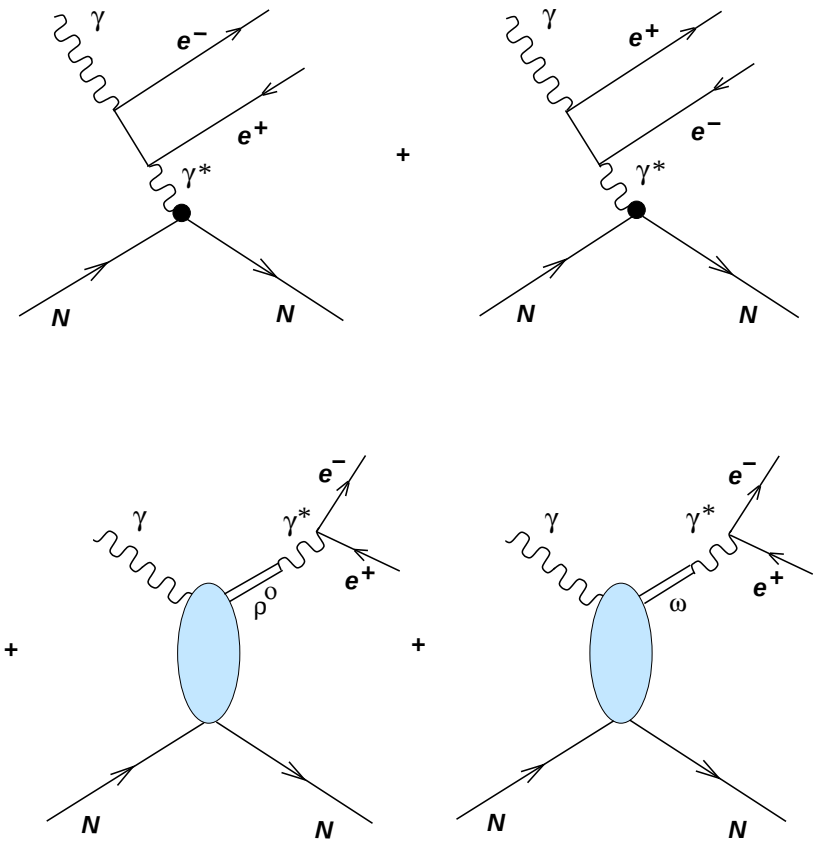

Fig. 1. Bethe-Heitler and vector meson decay contributions to the $\gamma N \to e^+e^-N$ amplitude.

The differential cross section for the $\gamma N \to e^+e^-N$ reaction is therefore in general the sum of three terms associated with the Bethe-Heitler process, the vector meson e^+e^- decay and their interference respectively.

The amplitudes displayed in Fig. 1 are calculated in the center of mass reference frame. We use the same notations as in Ref. [9]. We denote the 4-momenta of the incident photon and nucleon by q and p and the 4-momenta of the outgoing electron, positron and nucleon by p_-, p_+ and $\bar{p}$ respectively.

The invariant mass of the e^+e^- pair is defined as $m_{e^+e^-}=|\bar{q}|=\sqrt{(p_-+p_+)^2}$. The total center of mass energy $\sqrt{s}$ is related to the total 4-momentum $w = p+q = \overline{p}+\overline{q}$ by $\sqrt{s}=\sqrt{w^2}$. The magnitudes of the initial and final nucleon 3-momenta as functions of $\sqrt{s}$, $\overline{q}^2$ and the nucleon mass M_N are given by

$$|\vec{p}\,| \,=\, \frac{\sqrt{s}}{2}\left[1-\frac{M_N^2}{s}\right], \quad |\vec{\overline{p}}\,| \,=\, \frac{\sqrt{s}}{2}\left[1-2\,\frac{M_N^2+\overline{q}^2}{s}+\frac{(M_N^2-\overline{q}^2)^2}{s^2}\right]^{\frac{1}{2}}. \quad (1)$$

The differential cross section for the $\gamma N \to e^+e^-N$ reaction in the center of mass reference frame reads

$$\left[\frac{d\sigma}{d\overline{q}^2}\right]_{\gamma N\to e^+e^-N} = \frac{M_N^2}{32\pi^2 s}\,\frac{|\vec{\overline{p}}\,|}{|\vec{p}\,|}\int\frac{d^3\vec{p}_+}{(2\pi)^3}\,\frac{m_e}{p_+^0}\int\frac{d^3\vec{p}_-}{(2\pi)^3}\,\frac{m_e}{p_-^0}\,(2\pi)^4\,\delta^4(\overline{q}-p_+-p_-)$$
$$\sum_{\lambda_\gamma,\lambda,\overline{\lambda},\lambda_+,\lambda_-}\left|\mathcal{M}_{\gamma N\to e^+e^-N}(q,\lambda_\gamma,p,\lambda;p_+,\lambda_+,p_-,\lambda_-,\overline{p},\overline{\lambda})\right|^2, \quad (2)$$

where m_e denotes the electron mass.

The reaction matrix element $\mathcal{M}_{\gamma N\to e^+e^-N}$ is written as a sum of the Bethe-Heitler amplitudes, $\mathcal{M}^{BH}$, and amplitudes describing e^+e^- pair production via virtual ρ^0- and ω-mesons. The latter factorize into vector meson production and e^+e^- decay amplitudes. We have

$$\begin{aligned}
&\mathcal{M}_{\gamma N\to e^+e^-N}\,(q,\lambda_\gamma,p,\lambda;p_+,\lambda_+,p_-,\lambda_-,\overline{p},\overline{\lambda})\\
&\quad=\mathcal{M}^{BH}_{\gamma N\to e^+e^-N}(q,\lambda_\gamma,p,\lambda;p_+,\lambda_+,p_-,\lambda_-,\overline{p},\overline{\lambda})\\
&\quad+\mathcal{M}^{\mu}_{\gamma N\to \rho^0 N}(q,\lambda_\gamma,p,\lambda;\overline{q},\overline{p},\overline{\lambda})\;\mathcal{M}_{\rho^0\to e^+e^-,\mu}\,(\overline{q}\,;p_+,\lambda_+,p_-,\lambda_-)\\
&\quad+\mathcal{M}^{\mu}_{\gamma N\to \omega N}(q,\lambda_\gamma,p,\lambda;\overline{q},\overline{p},\overline{\lambda})\;\mathcal{M}_{\omega\to e^+e^-,\mu}\,(\overline{q}\,;p_+,\lambda_+,p_-,\lambda_-)\,, \qquad (3)
\end{aligned}$$

where the functional dependence on 4-momenta and polarization variables is made explicit.

The Bethe-Heitler amplitudes are sensitive to the electromagnetic structure of the target nucleon. They can be expressed in terms of the Dirac and Pauli form factors $F_1(t)$ and $F_2(t)$ where t is defined as $t \equiv (\overline{p}-p)^2$. In view of the kinematics involved in the present calculation ($1.4 < \sqrt{s} < 1.8$ GeV), our results will be sensitive to low values of t ($|t| < 1$ GeV^2). Furthermore the Bethe-Heitler process depends very dominantly on the particular combination $F_1(t)+F_2(t)$, i.e. on the magnetic form factor $G_M(t)$. In the kinematic range of interest, $G_M(t)$ has been measured accurately for both the proton and the neutron [13] and can be very well approximated by a dipole form.

We use for the Dirac and Pauli form factors the parametrization,

$$
\begin{aligned}
F_1^{(p)}(t) &= \frac{4\,M_p^2 - \mu_p\,t}{(1 - t/0.71\,[\mathrm{GeV}^{-2}])^2}\,\frac{1}{4\,M_p^2 - t}\,,\\
F_2^{(p)}(t) &= \frac{\mu_p - 1}{(1 - t/0.71\,[\mathrm{GeV}^{-2}])^2}\,\frac{4\,M_p^2}{4\,M_p^2 - t}\,,\\
F_1^{(n)}(t) &= \frac{-(\mu_n + 1 + t/2M_n^2)}{(1 - t/0.71\,[\mathrm{GeV}^{-2}])^2}\,\frac{t}{4\,M_n^2 - t}\,,\\
F_2^{(n)}(t) &= \frac{\mu_n + (t/4M_n^2)(1 + t/2M_n^2)}{(1 - t/0.71\,[\mathrm{GeV}^{-2}])^2}\,\frac{4\,M_n^2}{4\,M_n^2 - t}\,,
\end{aligned}
\tag{4}
$$

with $\mu_p = 2.793$ and $\mu_n = -1.913$. The corresponding proton and neutron electric and magnetic form factors read

$$
\begin{aligned}
G_E^{(p)}(t) &= \frac{1}{(1 - t/0.71\,[\mathrm{GeV}^{-2}])^2},\\
G_M^{(p)}(t) &= \frac{\mu_p}{(1 - t/0.71\,[\mathrm{GeV}^{-2}])^2},\\
G_E^{(n)}(t) &= \frac{(1 + t/2M_n^2)}{(1 - t/0.71\,[\mathrm{GeV}^{-2}])^2}\,\frac{-t}{4\,M_n^2}\,,\\
G_M^{(n)}(t) &= \frac{\mu_n}{(1 - t/0.71\,[\mathrm{GeV}^{-2}])^2}.
\end{aligned}
\tag{5}
$$

The Bethe-Heitler amplitudes factorize into the pair emission process by the incident photon and the target nucleon electromagnetic current transition matrix element and read [14]

$$
\begin{aligned}
&\mathcal{M}^{BH}_{\gamma N\to e^+e^-N}(q,\lambda_\gamma,p,\lambda;p_+,\lambda_+,p_-,\lambda_-,\overline{p},\overline{\lambda}) = \frac{e^3}{t}\,\varepsilon_\mu(q,\lambda_\gamma)\\
&\bar{u}(p_-,\lambda_-)\,\{\gamma^\mu\,\frac{-\not{q} + \not{p}_- + m_e}{-2\,q\cdot p_-}\,\gamma^\nu + \gamma^\nu\,\frac{\not{q} - \not{p}_+ + m_e}{-2\,q\cdot p_+}\,\gamma^\mu\}\,v(p_+,\lambda_+)\\
&\bar{u}(\overline{p},\overline{\lambda})\,\{\gamma_\nu F_1^{(N)}(t) - \frac{i}{2M_N}F_2^{(N)}(t)\,\sigma_{\nu\alpha}(p-\overline{p})^\alpha\}\,u(p,\lambda).
\end{aligned}
\tag{6}
$$

The vector meson photoproduction amplitudes entering Eq. (3), $\mathcal{M}^\mu_{\gamma N\to\rho^0 N}$ and $\mathcal{M}^\mu_{\gamma N\to\omega N}$, are calculated in the framework of the relativistic and unitary coupled-channel approach to meson-nucleon scattering of Ref. [7]. This description aims at a comprehensive description of data on pion-nucleon elastic and inelastic scattering and on meson photoproduction off nucleons in the energy window $1.4 < \sqrt{s} < 1.8$ GeV. It involves the πN, $\pi\Delta$, ρN, ωN, $K\Lambda$, $K\Sigma$,

ηN and γN channels. The fundamental fields are the mesons, the photon, the nucleon and the Δ-resonance (i.e. the baryons belonging to the octet and decuplet ground states). The meson-baryon scattering amplitudes are computed by solving coupled-channel Bethe-Salpeter equations. The Bethe-Salpeter kernel is constructed from an effective, quasi-local meson-meson-baryon-baryon Lagrangian among the fundamental fields. The coupling constants entering the effective Lagrangian are parameters which are adjusted to reproduce the data. In view of the kinematics, only s-wave scattering in the ρN and ωN channels is included, restricting πN and $\pi\Delta$ scattering to s- and d-waves. The pion-nucleon resonances in the S_{11}, S_{31}, D_{13} and D_{33} partial waves are generated dynamically by coupled-channel interactions [7]. These states correspond to the nucleon resonances $N^*_{3/2^-1/2}(1520)$, $N^*_{1/2^-1/2}(1535)$ and $N^*_{1/2^-1/2}(1650)$ and to the $\Delta_{1/2^-3/2}(1620)$ and $\Delta_{3/2^-3/2}(1700)$ isobars. In order to describe photon-nucleon and pion-nucleon data consistently, a generalized Vector Meson Dominance is introduced to relate amplitudes involving photons to amplitudes involving vector mesons. This prescription to extrapolate from real photons to vector mesons on the mass-shell is required to include the data on pion photoproduction multipole amplitudes which provide essential constraints on the effective Lagrangian parameters [7].

The $\gamma N \to \rho N$ and $\gamma N \to \omega N$ amplitudes in the generalized Vector Dominance approach of Ref. [7] are represented diagrammatically in Fig. 2.

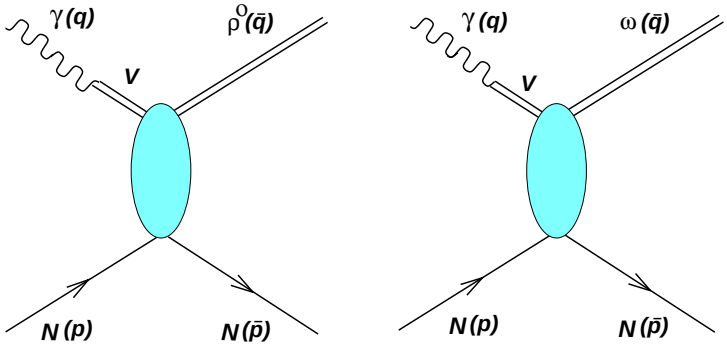

Fig. 2. Vector meson photoproduction amplitudes in the generalized Vector Dominance approach of Ref. [7].

The photon induced vector meson production amplitudes are determined by the $VN \to V'N$ scattering amplitudes with V or $V' = (\rho^0, \omega)$. The invariant transition matrix elements for the $VN \to V'N$ processes are given by

$$\langle V'^j(\overline{q})\, N(\overline{p})|\, \mathcal{T}\, |V^i(q)\, N(p)\rangle = (2\pi)^4\, \delta^4(q+p-\overline{q}-\overline{p}) \times \overline{u}(\overline{p})\, \epsilon^{\dagger\,\mu}_{V'}\,(\overline{q})\, T^{i,j}_{(VN\to V'N)\mu\nu}\, \epsilon^{\nu}_{V}(q)\, u(p), \quad (7)$$

where $T^{i,j}_{(VN\to V'N)\mu\nu}$ is a function of the three kinematic variables w, q and $\overline{q}$. Following the procedure of Ref. [9], we decompose the scattering amplitudes into isospin invariant components using the projectors defined in [15]. We get

$$\begin{aligned}\langle [V'(\overline{q})\, N(\overline{p})]_I |\, \mathcal{T}\, | [V(q)\, N(p)]_I \rangle = {} & (2\pi)^4\, \delta^4(q+p-\overline{q}-\overline{p}) \\ & \times \overline{u}(\overline{p})\, \epsilon^{\dagger\mu}_{V'}(\overline{q})\, T^{(I)}_{(VN\to V'N)\mu\nu}\, \epsilon^{\nu}_{V}(q)\, u(p). \quad (8)\end{aligned}$$

The eigenstates of the $[VN]$ system with total isospin I=1/2 and I=3/2 are related to the charge states of interest by

$$\begin{aligned}|\rho^{(0)} p\rangle &= +\sqrt{\tfrac{1}{3}}\, |[\rho N]_{I=1/2}\rangle + \sqrt{\tfrac{2}{3}}\, |[\rho N]_{I=3/2}\rangle\,, \\ |\rho^{(0)} n\rangle &= -\sqrt{\tfrac{1}{3}}\, |[\rho N]_{I=1/2}\rangle + \sqrt{\tfrac{2}{3}}\, |[\rho N]_{I=3/2}\rangle\,, \\ |\omega\, p\rangle &= |[\omega\, N]_{I=1/2}\rangle = |\omega\, n\rangle\,. \end{aligned} \quad (9)$$

The vector-meson nucleon scattering amplitudes $T^{(I)}_{(VN\to V'N)\,\mu\nu}(\overline{q}, q; w)$ are decomposed further into components of total angular momentum using the relativistic projection operators introduced in Ref. [15]. Because our model is restricted to s-wave vector-meson nucleon final states, this expansion takes the simple form,

$$\begin{aligned}T^{(I)}_{(VN\to V'N)\,\mu\nu}(\overline{q}, q; w) &= \sum_{J=1/2,3/2} P^{(J)}_{\mu\nu}\, M^{(I,J)}_{V\,N\to V'\,N}(s), \\ P^{(1/2)}_{\mu\nu} &= V_\mu\, P_-\, V_\nu\,, \quad P^{(3/2)}_{\mu\nu} = \Big(g_{\mu\nu} - \frac{w_\mu\, w_\nu}{w^2}\Big)\, P_+ - V_\mu\, P_-\, V_\nu\,, \end{aligned} \quad (10)$$

where $w_\mu = q_\mu + p_\mu = \bar{q}_\mu + \bar{p}_\mu$ and

$$V_\mu = \frac{1}{\sqrt{3}}\Big(\gamma_\mu - \frac{w_\mu}{w^2}\not{w}\Big)\,, \quad P_\pm = \frac{1}{2}\Big(1 \pm \frac{\not{w}}{\sqrt{w^2}}\Big)\,. \quad (11)$$

The invariant amplitudes $M^{(IJ)}_{VN\to V'N}(\sqrt{s})$ relevant for s-wave vector meson nucleon scattering are given and discussed in [7].

Following the approach of Ref. [7], the photon induced vector meson production amplitudes are related to the vector meson scattering amplitudes by the generalized Vector Meson Dominance assumption,

$$
\begin{aligned}
T^{\mu\nu}_{(\gamma\, p\to V\, p)} &= |e|\,\Big[T^{\mu\alpha}_{(\omega\, p\to V\, p)}(\bar{q},q;w)\,\Gamma^{\alpha\nu,+}_{\omega}(q,w) \\
&\quad + T^{\mu\alpha}_{(\rho^0\, p\to V\, p)}(\bar{q},q;w)\,\Gamma^{\alpha\nu,+}_{\rho}(q,w)\Big], \\
T^{\mu\nu}_{(\gamma\, n\to V\, n)} &= |e|\,\Big[T^{\mu\alpha}_{(\omega\, n\to V\, n)}(\bar{q},q;w)\,\Gamma^{\alpha\nu,+}_{\omega}(q,w) \\
&\quad - T^{\mu\alpha}_{(\rho^0\, n\to V\, n)}(\bar{q},q;w)\,\Gamma^{\alpha\nu,+}_{\rho}(q,w)\Big]\,,
\end{aligned}
\tag{12}
$$

where the positive parity transition tensor $\Gamma^{\mu\nu,+}_{\omega(\rho)}$ is constructed to achieve consistency with electromagnetic gauge invariance and reads

$$
\begin{aligned}
\Gamma^{\mu\nu,+}_{\omega(\rho)}(q,w) &= \frac{g^{(+)}_{\omega(\rho),1}}{M_\omega}\,P_+\left(\left(\not{q}-\frac{w\cdot q}{w^2}\not{w}\right)g^{\mu\nu}-q^\mu\left(\gamma^\nu-\frac{w^\nu}{w^2}\not{w}\right)\right) \\
&\quad + \frac{g^{(+)}_{\omega(\rho),2}}{M_\omega}\,P_+\left(\frac{w\cdot q}{\sqrt{w^2}}\,g^{\mu\nu}-\frac{q^\mu\,w^\nu}{\sqrt{w^2}}\right).
\end{aligned}
\tag{13}
$$

The coupling constants $g^{(+)}_{\omega(\rho),i}$ are determined by a fit to meson photoproduction data [7]. Their values are

$$
g^{(+)}_{\omega,1}=0.083,\qquad g^{(+)}_{\rho,1}=0.469,\qquad g^{(+)}_{\omega,2}=0.000,\qquad g^{(+)}_{\rho,2}=0.241. \tag{14}
$$

The vector meson photoproduction cross sections are fully described by the dimensionless and invariant amplitudes [7]

$$
\begin{aligned}
M^{(Jh)}_{\gamma\, p\to\rho^0\, p} &= \sqrt{N^{(\omega+)}_{Jh}}\,M^{(J)}_{\omega\, p\to\rho^0\, p}+\sqrt{N^{(\rho+)}_{Jh}}\,M^{(J)}_{\rho^0\, p\to\rho^0\, p}\,, \\
M^{(Jh)}_{\gamma\, n\to\rho^0\, n} &= \sqrt{N^{(\omega+)}_{Jh}}\,M^{(J)}_{\omega\, n\to\rho^0\, n}+\sqrt{N^{(\rho+)}_{Jh}}\,M^{(J)}_{\rho^0\, n\to\rho^0\, n}\,,
\end{aligned}
\tag{15}
$$

and similar expressions for $\gamma\, p\to\omega\, p$ and $\gamma\, n\to\omega\, n$, in which h is the helicity projection and the normalization factors are specific combinations of the coupling constants dependent on the kinematics [1]

$$
\begin{aligned}
\sqrt{N^{(\omega(\rho)+)}_{\frac{1}{2}\frac{1}{2}}} &= \frac{|e|}{M_\omega}\,\frac{|\vec{p}|}{\sqrt{6}}\,\left(2\left(\sqrt{s}-M_N\right)g^{(+)}_{\omega(\rho),1}+\left(\sqrt{s}+M_N\right)g^{(+)}_{\omega(\rho),2}\right), \\
\sqrt{N^{(\omega(\rho)+)}_{\frac{3}{2}\frac{1}{2}}} &= \frac{|e|}{M_\omega}\,\frac{|\vec{p}|}{\sqrt{24}}\,\left(-\left(\sqrt{s}-M_N\right)g^{(+)}_{\omega(\rho),1}+\left(\sqrt{s}+M_N\right)g^{(+)}_{\omega(\rho),2}\right), \\
\sqrt{N^{(\omega(\rho)+)}_{\frac{3}{2}\frac{3}{2}}} &= \frac{|e|}{M_\omega}\,\frac{|\vec{p}|}{\sqrt{8}}\,\left(\left(\sqrt{s}-M_N\right)g^{(+)}_{\omega(\rho),1}+\left(\sqrt{s}+M_N\right)g^{(+)}_{\omega(\rho),2}\right),
\end{aligned}
\tag{16}
$$

[1] Note that the normalization factors N introduced here differ from corresponding terms used in [7] by a factor $s^{1/4}$.

with $\sqrt{s} = |\vec{p}| + \sqrt{M_N^2 + \vec{p}^2}$. Since the amplitudes introduced in (15) determine the dilepton photoproduction cross sections, we display them in Fig. 3.

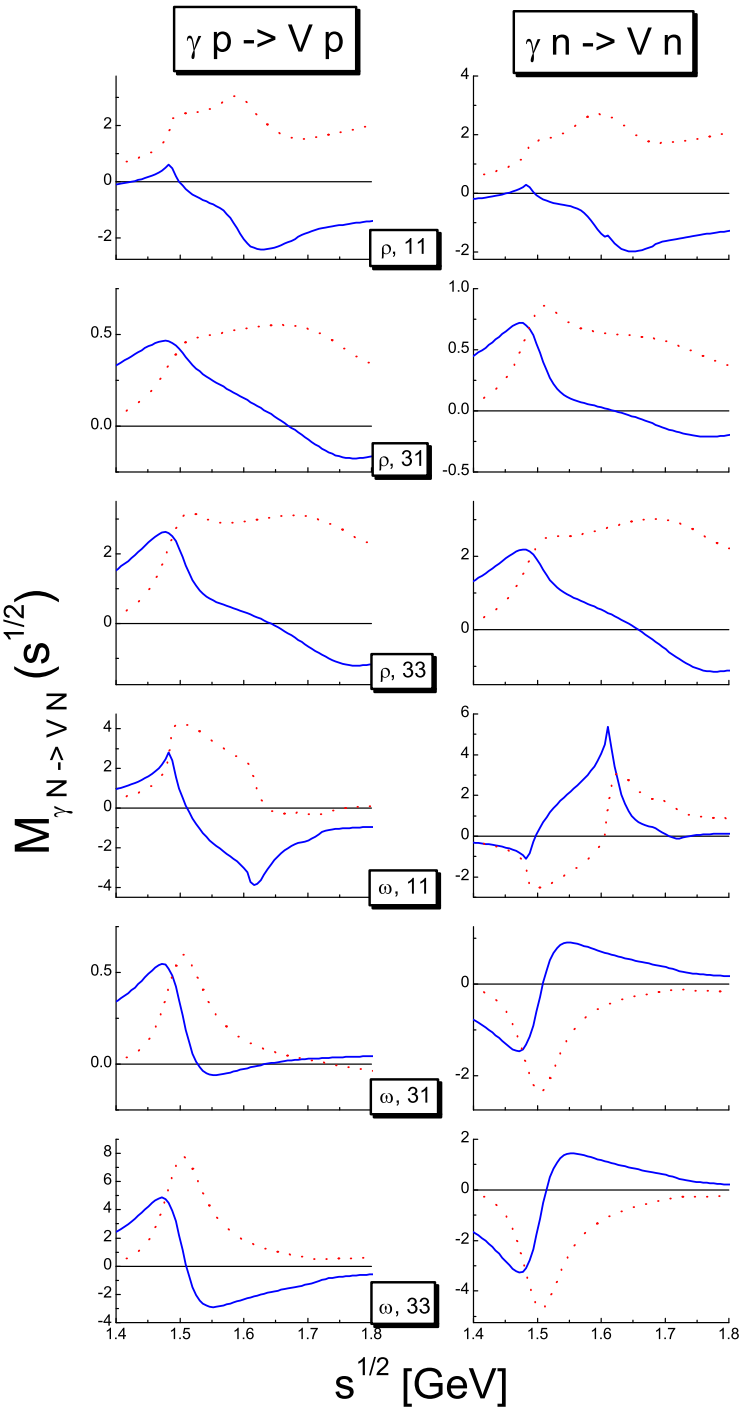

Fig. 3. The $\gamma N \to VN$ amplitudes with $V = (\rho^0, \omega)$ and $N = (p, n)$ as defined in Eq. (15). The indices $11, 31, 33$ specify the total angular momentum $2J$ and the helicity projection $2h$ with $(J, h) = ((\frac{1}{2}, \frac{1}{2}), (\frac{3}{2}, \frac{1}{2}), (\frac{3}{2}, \frac{3}{2}))$ respectively. The solid lines indicate real parts and the dotted lines imaginary parts.

To derive $\gamma N \to e^+e^-N$ amplitudes from Eq. (15), we follow the same prescription as in Ref. [9]. We assume that the coupling of massive photons (materializing into e^+e^- pairs) to vector mesons is given by the Lagrangian

$$\mathcal{L}_{\gamma V}^{int} = \frac{f_\rho}{2\,M_\rho^2} F^{\mu\nu}\,\rho^0_{\mu\nu} \;+\; \frac{f_\omega}{2\,M_\omega^2} F^{\mu\nu}\,\omega_{\mu\nu}, \tag{17}$$

where the photon and vector meson field tensors are defined by

$$F^{\mu\nu} \;=\; \partial^\mu A^\nu - \partial^\nu A^\mu\,, \qquad V^{\mu\nu} \;=\; \partial^\mu V^\nu - \partial^\nu V^\mu. \tag{18}$$

In Eq. (17), f_ρ and f_ω are dimensional coupling constants. Their magnitude can be determined from the e^+e^- partial decay widths of the ρ- and ω-mesons to be [16]

$$|f_\rho| = 0.036\,\mathrm{GeV}^2\,, \qquad |f_\omega| = 0.011\,\mathrm{GeV}^2. \tag{19}$$

The relative sign of f_ρ and f_ω is fixed by vector meson photoproduction amplitudes [7]. With our sign conventions, f_ρ and f_ω are both positive.

We emphasize that the interaction Lagrangian (17) provides a satisfactory phenomenological description of the coupling of time-like photons to vector mesons [1] but does not give any contribution to the processes involving real photons. Implementing the Vector Meson Dominance assumption in the description of photoproduction processes required therefore the more general structure exhibited in Eq. (12). Our calculation of the $\gamma N \to e^+e^-N$ reaction is consequently valid for lepton pair masses sufficiently close to the vector meson masses, where the dilepton production cross section is dominated by the vector meson pole terms. It is important to remark that this range of applicability is compatible with the restriction to s-wave scattering for the $\rho^0 N$- and ωN-channels in the work of Ref. [7]. This restriction means indeed that this approach applies to final states where the time-like photon has little relative motion with respect to the nucleon, i. e. to the e^+e^- pairs with the largest invariant masses allowed by the reaction kinematics.

3 Calculation of the $\gamma p \to e^+e^-p$ and $\gamma n \to e^+e^-n$ cross sections

Using the Bethe-Heitler and vector meson amplitudes described in the previous section, we can proceed to the calculation of differential cross sections for the $\gamma p \to e^+e^-p$ and $\gamma n \to e^+e^-n$ reactions.

The e^+e^- pair produced in the final state is characterized by the electron and positron 3-momenta $\vec{p}_-$ and $\vec{p}_+$. The reduction of these six variables with the aim of exhibiting the physics of interest in the $\gamma N \to e^+e^-N$ reactions is an important issue.

If the leptonic phase space is fully integrated out, the interference terms between the Bethe-Heitler and vector meson amplitudes cancel. This is a consequence of Furry's theorem [17] which states that Feynman diagrams containing a closed fermion loop with an odd number of photon vertices do not contribute to physical processes because the two orientations of the loop lead to identical terms of opposite sign. The fully integrated dilepton mass spectra, $d\sigma/dm^2_{e^+e^-}$, are therefore the incoherent sums of Bethe-Heitler pair and vector meson production processes. In view of the smallness of the cross sections it is likely that these mass spectra will be the first measurements available close to the vector meson production threshold. Because the Bethe-Heitler cross section can be calculated accurately, they provide access to the vector meson production terms and in particular to the ρ^0-ω interference in the e^+e^- channel. This interference pattern is the quantity of interest to study the excitation of baryon resonances through vector fields. We remark that the incoherent sum of Bethe-Heitler and vector meson contributions in the $\gamma N \to e^+e^-N$ reaction is symmetric under the exchange of the electron and positron momenta. It can be determined experimentally by measuring this process without distinguishing the positron and the electron in the final state as emphasized in Ref. [18]. Another technique, used many years ago at DESY [19] for high energy incident photons scattered diffractively, is to detect e^+e^- pairs symmetrically around the beam axis.

The interference of Bethe-Heitler pairs with e^+e^- pairs produced by the decay of vector mesons reflects in asymmetries [20,21]. They are defined by subdividing the lepton pair phase space into two hemispheres. Let us consider first the rest frame of the produced e^+e^- pair. We call forward and backward electrons those characterized by $\cos(\vec{p}_-, \vec{q}) > 0$ and $\cos(\vec{p}_-, \vec{q}) < 0$ respectively. If the e^+e^- pair is moving, the $\vec{p}_-.\vec{q}$ product can be generalized naturally by the Lorentz invariant quantity $\frac{1}{2}q(p_+ - p_-)$. We can then project the cross section onto the forward and backward hemispheres using the θ functions, $\theta[+q(p_+ - p_-)]$ and $\theta[-q(p_+ - p_-)]$. We refer to these projections as σ^+ and σ^-. The backward hemisphere is clearly obtained from the forward hemisphere by interchanging the electron and positron momenta. We choose as angular

variable the scattering angle θ of the lepton pair (or equivalently the Mandelstam variable $t = (\bar{q} - q)^2$). This variable will prove very useful to distinguish pairs arising from Bethe-Heitler and vector meson production processes.

The sum of the doubly differential cross sections

$$\left[\frac{d\,\sigma^{sym}}{d\,\overline{q}^2\,d\,t}\right]_{\gamma\,N\to e^+e^-N} = \left[\frac{d\,\sigma^{+}}{d\,\overline{q}^2\,d\,t}\right]_{\gamma\,N\to e^+e^-N} + \left[\frac{d\,\sigma^{-}}{d\,\overline{q}^2\,d\,t}\right]_{\gamma\,N\to e^+e^-N}, \qquad (20)$$

is symmetric for the interchange of the electron and positron momenta and contains no interference of Bethe-Heitler pairs with e^+e^- pairs from vector meson decays. This interference is given by the difference

$$\left[\frac{d\,\sigma^{asym}}{d\,\overline{q}^2\,d\,t}\right]_{\gamma\,N\to e^+e^-N} = \left[\frac{d\,\sigma^{+}}{d\,\overline{q}^2\,d\,t}\right]_{\gamma\,N\to e^+e^-N} - \left[\frac{d\,\sigma^{-}}{d\,\overline{q}^2\,d\,t}\right]_{\gamma\,N\to e^+e^-N}, \qquad (21)$$

expressing the property that it is antisymmetric under the interchange of the electron and positron momenta as a consequence of the opposite charge conjugation parity of the Bethe-Heitler and vector meson decay amplitudes [20,21]. This effect was used to measure the quantum interference of Bethe-Heitler pairs and e^+e^- pairs from vector meson decays at high energy, using a two-arm spectrometer with right and left arms positioned at different angles with respect to the beam direction [22].

In the center of mass reference frame, the differential cross sections for the $\gamma\,p \to e^+e^-p$ reaction projected onto the forward and backward hemispheres are given by

$$\left[\frac{d\,\sigma^{\pm}}{d\,\overline{q}^2\,d\,\cos\theta}\right]_{\gamma\,p\to e^+e^-p} = \frac{M_p^2}{64\,\pi^2 s}\,\frac{|\vec{\overline{p}}\,|}{|\vec{p}\,|}\int\frac{d^3\vec{p}_+}{(2\pi)^3}\,\frac{m_e}{p_+^0}\int\frac{d^3\vec{p}_-}{(2\pi)^3}\,\frac{m_e}{p_-^0}$$
$$\times\sum_{\lambda,\overline{\lambda},\lambda_\gamma,\lambda_+,\lambda_-}|\mathcal{M}_{\gamma\,p\to e^+e^-p}|^{\,2}\theta\,[\,\pm\,q\cdot(p_+ - p_-)]\,(2\pi)^4\,\delta^4(\overline{q} - p_+ - p_-). \qquad (22)$$

The relation between the covariant double differential cross sections of Eqs. (20, 21) and the angular distributions (22) reads simply

$$\frac{d\,\sigma^{\pm}}{d\,\bar{q}^2 d\,t} = \frac{1}{2\,|\vec{p}\,|\,|\vec{\overline{p}}\,|}\,\frac{d\,\sigma^{\pm}}{d\,\bar{q}^2 d\cos\theta}\,. \qquad (23)$$

Performing the integrations over the lepton phase space and summing over initial and final polarizations, we obtain

$$\Big[\frac{d\,\sigma^{\pm}}{d\,\overline{q}^2\,d\,\cos\theta}\Big]_{\gamma\,p\to e^+e^-p} = \frac{\alpha}{\pi^2}\,\frac{M_p^2}{64\,s}\,\frac{|\vec{\overline{p}}\,|}{|\vec{p}\,|}\,\sqrt{1-\frac{4\,m_e^2}{\overline{q}^2}}\,\Bigg(\frac{|e|^2}{t^2}\,C_{\rm BH}$$
$$+\sum_{V,V'J,J',h}\,\frac{f_V}{M_V^2}\,\frac{f_{V'}}{M_{V'}^2}\,C_{\rm VM}^{(JJ',h)}\,M_{\gamma\,p\to V\,p}^{(Jh)}\,S_V(\bar{q}^2)\,M_{\gamma\,p\to V'\,p}^{\dagger(J'h)}\,S_{V'}^{\dagger}(\bar{q}^2)$$
$$\pm\sum_{V,J,h}\,\frac{|e|\,f_V}{M_V^2\,t}\,C_{\rm asym}^{(Jh)}\,\Big(M_{\gamma\,p\to V\,p}^{\dagger(Jh)}\,S_V^{\dagger}(\bar{q}^2)+M_{\gamma\,p\to V\,p}^{(Jh)}\,S_V(\bar{q}^2)\Big)\Bigg)\,, \qquad (24)$$

where the symbols S_V stand for the vector meson propagators,

$$S_\rho(\overline{q}^2)\,\equiv\,\frac{1}{\overline{q}^2-M_\rho^2+i\Gamma_\rho(\overline{q}^2)\,M_\rho}\,,\qquad S_\omega(\overline{q}^2)\,\equiv\,\frac{1}{\overline{q}^2-M_\omega^2+i\Gamma_\omega\,M_\omega}, \qquad (25)$$

with the energy-dependent ρ-width given by

$$\Gamma_\rho(\overline{q}^2)\,=\,\Gamma_\rho\,\frac{M_\rho}{\sqrt{\overline{q}^2}}\,\Big(\frac{\overline{q}^2-4\,m_\pi^2}{M_\rho^2-4\,m_\pi^2}\Big)^{\frac{3}{2}}. \qquad (26)$$

Γ_ρ and Γ_ω denote the widths at the peak of the ρ and ω resonances. The invariant production amplitudes $M_{\gamma\,p\to V\,p}^{(Jh)}$ were introduced and discussed in the previous section. The set of dimensionless functions $C_{\rm BH}, C_{\rm VM}$ and $C_{\rm asym}$ are of kinematical origin and do not contain any dynamical information but the electromagnetic form factors of the proton. Their derivation is discussed in the Appendix.

The coefficient $C_{\rm BH}$ represents the Bethe-Heitler pair production mechanism in accordance with the early work of Drell and Walecka [14] and reads

$$C_{\rm BH}=\frac{|e|^2\,|F_1^{(p)}(t)+F_2^{(p)}(t)|^2}{M_p^2\,(\bar{q}^2-t)^2}\Big((\bar{q}^2)^2+t^2\Big)\,\Big(t-2\,t\,{\rm arcth}\,\sqrt{1-\frac{4\,m_e^2}{\bar{q}^2}}\,\Big)$$
$$-\,4\,\frac{|e|^2\,(|F_1^{(p)}(t)|^2-\frac{t}{4\,M_p^2}\,|F_2^{(p)}(t)|^2)}{M_p^2\,(\bar{q}^2-t)^4}\,\Bigg((M_p^4\,t+s\,t\,(-\bar{q}^2+s+t)$$
$$+M_p^2\,\Big((\bar{q}^2)^2-(\bar{q}^2+2\,s)\,t\Big)\Big)\,\Big((\bar{q}^2)^2+t^2\Big)\,{\rm arcth}\,\sqrt{1-\frac{4\,m_e^2}{\bar{q}^2}}$$
$$+\,2\,\frac{|e|^2\,(|F_1^{(p)}(t)|^2-\frac{t}{4\,M_p^2}\,|F_2^{(p)}(t)|^2)}{M_p^2\,(\bar{q}^2-t)^4}\,\Bigg((\bar{q}^2)^2\,(M_p^2-s)\,(M_p^2+\bar{q}^2-s)\,t$$
$$+\bar{q}^2\,\Big(6\,M_p^4+3\,M_p^2\,(\bar{q}^2-4\,s)+(\bar{q}^2-3\,s)\,(\bar{q}^2-2\,s)\Big)\,t^2$$
$$+\Big(M_p^4-2\,(\bar{q}^2)^2+5\,\bar{q}^2\,s+s^2-M_p^2\,(5\,\bar{q}^2+2\,s)\Big)\,t^3$$
$$+M_p^2\,(\bar{q}^2)^4+(\bar{q}^2+s)\,t^4\Bigg)+\mathcal{O}\left(m_e^2\right). \qquad (27)$$

The coefficients $C_{\rm VM}^{(JJ',h)}$ contain the contribution of the square of the sum of the vector meson photoproduction amplitudes to the lepton pair production cross section. As suggested by Eq. (24), there are many terms reflecting interference effects among amplitudes with different total angular momenta J and J' in the vector meson-nucleon channel as well as the interfering $\rho^0 p \to e^+\, e^- p$ and $\omega p \to e^+\, e^- p$ final states. We have

$$
\begin{aligned}
C_{\rm VM}^{(\frac{1}{2}\frac{1}{2},\frac{1}{2})} &= \frac{(M_p+\sqrt{s}\,)^2-\bar{q}^2}{144\,M_p^2\,\bar{q}^2\,s^2}\left(\bar{q}^2+2\,m_e^2\right)\Bigg(M_p^4+(\bar{q}^2)^2 \\
&\quad +10\,\bar{q}^2\,s+s^2-2\,M_p^2\,(\bar{q}^2+s^2)\Bigg)\,, \\
C_{\rm VM}^{(\frac{3}{2}\frac{3}{2},\frac{1}{2})} &= \frac{(M_p+\sqrt{s}\,)^2-\bar{q}^2}{36\,M_p^2\,(s-M_p^2)^2\,s^2\,\bar{q}^2}\left(\bar{q}^2+2\,m_e^2\right)\Bigg(M_p^8-2\,M_p^6\,(\bar{q}^2+2\,s) \\
&\quad -2\,M_p^2\,s^2\left((\bar{q}^2)\,(\bar{q}^2+8\,s)+2\,s^2-3\,(q\cdot\bar{q})\,(\bar{q}^2+2\,s)\right) \\
&\quad +s^2\left(12\,(q\cdot\bar{q})^2+(\bar{q}^2)^2+7\,\bar{q}^2\,s^2+s^2-6\,(q\cdot\bar{q})\,(\bar{q}^2+s^2)\right) \\
&\quad +M_p^4\left((\bar{q}^2)^2+(-6\,q\cdot\bar{q}+11\,\bar{q}^2)\,s^2+6\,s^2\right)\Bigg)\,, \\
C_{\rm VM}^{(\frac{3}{2}\frac{3}{2},\frac{3}{2})} &= \frac{(M_p+\sqrt{s}\,)^2-\bar{q}^2}{12\,M_p^2\,(s-M_p^2)^2\,s\,\bar{q}^2}\left(\bar{q}^2+2\,m_e^2\right)\Bigg(M_p^4\,(2\,q\cdot\bar{q}+\bar{q}^2) \\
&\quad -2\left(2\,(q\cdot\bar{q})\,(M_p^2+q\cdot\bar{q})+(M_p^2-q\cdot\bar{q})\,\bar{q}^2\right)s \\
&\quad +(2\,q\cdot\bar{q}+\bar{q}^2)\,s^2-2\,M_p^2\,(q\cdot\bar{q})\,\bar{q}^2\Bigg)\,, \\
C_{\rm VM}^{(\frac{1}{2}\frac{3}{2},\frac{1}{2})} &= \frac{(M_p+\sqrt{s}\,)^2-\bar{q}^2}{72\,M_p^2\,(s-M_p^2)^2\,s^2\,\bar{q}^2}\left(\bar{q}^2+2\,m_e^2\right)\Bigg(-M_p^4\,(M_p^2-\bar{q}^2)^2 \\
&\quad +2\,M_p^2\left(2\,M_p^4+M_p^2\,(6\,q\cdot\bar{q}-4\,\bar{q}^2)+\bar{q}^2\,(-6\,q\cdot\bar{q}+\bar{q}^2)\right)s \\
&\quad -\Big(6\,(M_p^2+2\,q\cdot\bar{q})^2-2\,(5\,M_p^2+6\,q\cdot\bar{q})\,\bar{q}^2+(\bar{q}^2)^2\Big)\,s^2 \\
&\quad +4\,(M_p^2+3\,q\cdot\bar{q}-\bar{q}^2)\,s^3-s^4\Bigg)\,. \qquad (28)
\end{aligned}
$$

The dependence on the center of mass scattering angle θ is contained in the $q\cdot\bar{q}$ product according to

$$
q\cdot\bar{q}=p\,\sqrt{\bar{q}^2+\bar{p}^2}-p\,\bar{p}\,\cos\theta\,. \qquad (29)
$$

The kinematical functions $C_{\rm VM}^{(JJ',h)}$ are symmetric under the exchange of the indices J and J'. Properly averaged over the scattering angle θ, they vanish identically for $J\neq J'$.

The coefficient functions $C_{\rm asym}^{(Jh)}$ characterize the kinematics of the interference among the vector meson and the Bethe-Heitler terms. They read

$$
\begin{aligned}
C_{\rm asym}^{(\frac{1}{2}\frac{1}{2})} = & \frac{|e|\,F_1(t)}{8\sqrt{6}\,M_p^2\,(s-M_p^2)\,(\bar{q}^2-t)^3\,s}\,\Big(-M_p^6\,t^2\,(3\,\bar{q}^2+t) \\
& -2\,M_p^5\,\sqrt{s}\,t\,\Big(-2\,(\bar{q}^2)^2+\bar{q}^2\,t+t^2\Big) \\
& +2\,M_p^3\,\sqrt{s}\,(\bar{q}^2-t)\,\Big((\bar{q}^2)^3-\bar{q}^2\,(\bar{q}^2+4\,s)\,t-2\,s\,t^2\Big) \\
& +M_p^4\,t\,\Big(-2\,(\bar{q}^2)^2\,(\bar{q}^2-2\,s)+\bar{q}^2\,(\bar{q}^2+7\,s)\,t+(\bar{q}^2+s)\,t^2\Big) \\
& -M_p\,\sqrt{s}\,(\bar{q}^2-t)\,\Big((\bar{q}^2)^3\,(\bar{q}^2-2\,t)-2\,s^2\,t^2 \\
& +\bar{q}^2\,(\bar{q}^2-2\,s)\,t\,(2\,s+t)\Big)+s^2\,t\,\Big(-3\,(\bar{q}^2)^3-t^2\,(s+t) \\
& +2\,(\bar{q}^2)^2\,(2\,s+t)+\bar{q}^2\,t\,(s+2\,t)\Big)+M_p^2\,s\,\Big((\bar{q}^2)^3\,(2\,\bar{q}^2-t) \\
& +(t-5\,\bar{q}^2)\,t^2\,(s+t)+(\bar{q}^2)^2\,t\,(-8\,s+3\,t)\Big)\Big) \\
& +\frac{|e|\,F_2(t)}{32\sqrt{6}\,M_p^3\,(\sqrt{s}+M_p)\,(\bar{q}^2-t)^3\,s}\,\Big(2\,M_p^6\,t^2\,(3\,\bar{q}^2+t) \\
& +4\,M_p^5\,\sqrt{s}\,t^2\,\Big(3\,\bar{q}^2+t\Big)+M_p^4\,t^2\,\Big(\bar{q}^2\,(\bar{q}^2-6\,s)-2\,(\bar{q}^2+s)\,t \\
& +t^2\Big)+4\,M_p^3\,\sqrt{s}\,t\,\Big((\bar{q}^2)^3-\bar{q}^2\,(\bar{q}^2+6\,s)\,t-(\bar{q}^2+2\,s)\,t^2 \\
& +t^3\Big)+M_p^2\,\Big(-2\,(\bar{q}^2)^5+(\bar{q}^2)^3\,(3\,\bar{q}^2+10\,s)\,t \\
& -\bar{q}^2\,((\bar{q}^2)^2+16\,\bar{q}^2\,s+6\,s^2)\,t^2+((\bar{q}^2)^2+2\,\bar{q}^2\,s-2\,s^2)\,t^3 \\
& -(\bar{q}^2-4\,s)\,t^4\Big)+2\,M_p\,\sqrt{s}\,t\,\Big(-3\,(\bar{q}^2)^4 \\
& +2\,s^2\,t^2-(\bar{q}^2)^2\,t\,(8\,s+t)+(\bar{q}^2)^3\,(4\,s+5\,t) \\
& +\bar{q}^2\,t\,(6\,s^2+4\,s\,t-t^2)\Big)+s\,t\,\Big(-2\,(\bar{q}^2)^4-(\bar{q}^2)^2\,t\,(5\,s+t) \\
& +(\bar{q}^2)^3\,(2\,s+3\,t)-t^2\,(-2\,s^2+s\,t+t^2) \\
& +\bar{q}^2\,t\,(6\,s^2+4\,s\,t+t^2)\Big)\Big)+\mathcal{O}\left(m_e^0\right)\,, \qquad (30)
\end{aligned}
$$

$$
\begin{aligned}
C_{\rm asym}^{(\frac{3}{2}\frac{1}{2})} = & \frac{|e|\,F_1(t)}{4\sqrt{6}\,M_p^2\,(s-M_p^2)^2\,(\bar{q}^2-t)^3\,s}\,\Big(-M_p^8\,t^2\,\Big(3\,\bar{q}^2+t\Big) \\
& +M_p^7\,\sqrt{s}\,t\,\Big(-2\,(\bar{q}^2)^2+\bar{q}^2\,t+t^2\Big) \\
& -M_p^5\,\sqrt{s}\,(\bar{q}^2-t)\,((\bar{q}^2)^3-2\,\bar{q}^2\,(2\,\bar{q}^2+3\,s)\,t+3\,(\bar{q}^2-s)\,t^2) \\
& +M_p^3\,\sqrt{s}\,(\bar{q}^2-t)\,((\bar{q}^2)^3\,(2\,\bar{q}^2+s)-2\,\bar{q}^2\,(2\,(\bar{q}^2)^2 \\
& +3\,\bar{q}^2\,s+3\,s^2)\,t+(2\,\bar{q}^2-s)\,(\bar{q}^2+3\,s)\,t^2) \\
& +M_p^6\,t\,(-2\,(\bar{q}^2)^2\,(\bar{q}^2+s)+\bar{q}^2\,(\bar{q}^2+13\,s)\,t
\end{aligned}
$$

$$
\begin{aligned}
&+(\bar{q}^2+5\,s)\,t^2)+M_p^2\,s^2\,((\bar{q}^2)^4+(\bar{q}^2)^2\,(\bar{q}^2-6\,s)\,t\\
&-5\,\bar{q}^2\,(2\,\bar{q}^2-3\,s)\,t^2+(4\,\bar{q}^2+7\,s)\,t^3+4\,t^4)\\
&-M_p^4\,s\,((\bar{q}^2)^4-4\,(\bar{q}^2)^3\,t-2\,(\bar{q}^2)^2\,t\,(3\,s+t)\\
&+3\,\bar{q}^2\,t^2\,(7\,s+t)+t^3\,(9\,s+2\,t))-s^3\,t\,(3\,(\bar{q}^2)^3\\
&+2\,t^2\,(s+t)+2\,\bar{q}^2\,t\,(2\,s+t)-(\bar{q}^2)^2\,(2\,s+7\,t))\\
&+M_p\,s^{3/2}\,(\bar{q}^2-t)\,((\bar{q}^2)^4-5\,(\bar{q}^2)^3\,t+s^2\,t^2\\
&+(\bar{q}^2)^2\,t\,(2\,s+7\,t)+\bar{q}^2\,t\,(2\,s^2-2\,s\,t-3\,t^2))\Big)\\
&+\frac{|e|\,F_2(t)\,(M_p+\sqrt{s})}{16\,\sqrt{6}\,M_p^3\,(s-M_p^2)^2\,(\bar{q}^2-t)^3\,s}\,\Big(2\,M_p^8\,t^2\,(3\,\bar{q}^2+t)\\
&-2\,M_p^5\,\sqrt{s}\,(\bar{q}^2-t)\,t\,((\bar{q}^2)^2-8\,\bar{q}^2\,t-2\,t^2)\\
&-M_p^3\,\sqrt{s}\,(\bar{q}^2-t)\,(2\,(\bar{q}^2)^4-(\bar{q}^2)^2\,(13\,\bar{q}^2+4\,s)\,t\\
&+8\,\bar{q}^2\,(\bar{q}^2+4\,s)\,t^2+(3\,\bar{q}^2+8\,s)\,t^3)+M_p^4\,(-2\,(\bar{q}^2)^5\\
&+(\bar{q}^2)^3\,(3\,\bar{q}^2+2\,s)\,t-\bar{q}^2\,((\bar{q}^2)^2+19\,\bar{q}^2\,s\\
&-36\,s^2)\,t^2+((\bar{q}^2)^2+14\,\bar{q}^2\,s+12\,s^2)\,t^3-(\bar{q}^2-3\,s)\,t^4)\\
&+M_p^6\,t^2\,((\bar{q}^2)^2+t\,(-8\,s+t)-2\,\bar{q}^2\,(12\,s+t))\\
&+M_p\,s^{3/2}\,(\bar{q}^2-t)\,t\,(7\,(\bar{q}^2)^3+4\,t^2\,(s+t)\\
&-2\,(\bar{q}^2)^2\,(s+11\,t)+\bar{q}^2\,t\,(16\,s+11\,t))\\
&+s^2\,t\,(-2\,(\bar{q}^2)^4+t^2\,(2\,s+t)\,(s+2\,t)\\
&+2\,\bar{q}^2\,t\,(s+t)\,(3\,s+2\,t)+2\,(\bar{q}^2)^3\,(s+6\,t)\\
&-(\bar{q}^2)^2\,t\,(17\,s+16\,t))+M_p^2\,s\,(-2\,(\bar{q}^2)^5+(\bar{q}^2)^4\,t\\
&+(\bar{q}^2)^2\,t^2\,(35\,s+t)+(\bar{q}^2)^3\,t\,(-4\,s+3\,t)\\
&-\bar{q}^2\,t^2\,(2\,s+t)\,(12\,s+5\,t)+t^3\,(-8\,s^2-9\,s\,t+2\,t^2))\Big)\\
&+\mathcal{O}\left(m_e^2\right), \qquad (31)
\end{aligned}
$$

$$
\begin{aligned}
C_{\rm asym}^{(\frac{3}{2}\frac{3}{2})} =& \frac{|e|\,F_1(t)}{4\,\sqrt{2}\,M_p^2\,(s-M_p^2)^2\,(\bar{q}^2-t)^2\,s^{1/2}}\\
&\times\Big(-M_p^3-M_p^2\,\sqrt{s}+M_p\,s+\sqrt{s}\,(-\bar{q}^2+s+t)\Big)\\
&\Big((M_p^4\,t\,(2\,\bar{q}^2+t)+s\,t\,((-\bar{q}^2)\,(\bar{q}^2-2\,s)+(\bar{q}^2+s)\,t)\\
&+M_p^2\,((\bar{q}^2)^3-\bar{q}^2\,(\bar{q}^2+4\,s)\,t-2\,s\,t^2))\Big)\\
&+\frac{|e|\,F_2(t)\,(M_p+\sqrt{s})}{16\,\sqrt{2}\,M_p^3\,(s-M_p^2)^2\,(\bar{q}^2-t)^2\,s^{1/2}}\,\Big(2\,M_p^4\,\sqrt{s}\,t^2\,(2\,\bar{q}^2+t)
\end{aligned}
$$

$$
\begin{aligned}
&-2\,M_p^5\,t\,((\bar{q}^2)^2+\bar{q}^2\,t+t^2)+M_p^2\,\sqrt{s}\,t\,(4\,(\bar{q}^2)^3-\bar{q}^2\,(3\,\bar{q}^2+8\,s)\,t\\
&-2\,(\bar{q}^2+2\,s)\,t^2+t^3)+M_p^3\,(-2\,(\bar{q}^2)^4+(\bar{q}^2)^2\,(\bar{q}^2+4\,s)\,t\\
&+4\,\bar{q}^2\,s\,t^2+(\bar{q}^2+4\,s)\,t^3)+M_p\,s\,t\,((\bar{q}^2)^3-2\,(\bar{q}^2)^2\,s\\
&+\bar{q}^2\,t\,(-2\,s+t)-2\,t^2\,(s+t))+s^{3/2}\,t^2\,(-3\,(\bar{q}^2)^2\\
&+2\,\bar{q}^2\,(2\,s+t)+t\,(2\,s+t))\Big)+\mathcal{O}\left(m_e^2\right)\,. \qquad (32)
\end{aligned}
$$

The derivation of the cross section in the other iospin channel, $\gamma\,n\to e^+e^-n$, is completely similar, with the obvious replacement of $\mathcal{M}_{\gamma\,p\to\rho^0 p}$ and $\mathcal{M}_{\gamma\,p\to\omega\,p}$ by $\mathcal{M}_{\gamma\,n\to\rho^0 n}$ and $\mathcal{M}_{\gamma\,n\to\omega\,n}$ and of $F_{1,2}^{(p)}$ by $F_{1,2}^{(n)}$.

4 Numerical results

We begin the presentation of our numerical results by displaying e^+e^- pair spectra where the leptonic phase space is fully integrated. As discussed earlier, there is no interference between Bethe-Heitler and vector meson decay amplitudes in that situation. We show first spectra at $\sqrt{s}$=1.75 and 1.65 GeV, i.e. just above and just below the ω-meson production threshold. These results are presented in Fig. 4 for the $\gamma\,p\to e^+e^-p$ reaction and in Fig. 5 for the $\gamma\,n\to e^+e^-n$ reaction. To unravel the dynamics of the dilepton production process, we display separately the Bethe-Heitler and vector meson decay contributions to the cross sections and the decomposition of the vector meson decay cross sections into the ρ, ω and ρ-ω interference terms for the two possible spin channels (J=1/2 and J=3/2).

We consider first the differential cross sections $\mathrm{d}\sigma/\mathrm{dm}^2_{e^+e^-}$ above threshold at $\sqrt{s}$=1.75 GeV. We see that they are dominated by the vector meson contribution in the region of interest ($0.7 < \mathrm{m}^{\,2}_{e^+e^-} < 0.8$ GeV), with cross sections of the order of a few nbarn per GeV^2. The pattern for proton and neutron targets is quite different. The origin of this effect is the quantum interference between ρ- and ω-meson e^+e^- decays. This interference is constructive for proton targets and destructive for neutron targets, particularly in the J=3/2 channel. This feature can be understood from the opposite signs of the $\gamma\,p\to\omega p$ and $\gamma\,n\to\omega n$ amplitudes in the (J,h)=(3/2,3/2) channel displayed in Fig. 3. We note also that the $\gamma\,N\to\omega N$ amplitudes are mostly real at threshold while the $\gamma\,N\to\rho N$ amplitudes have large imaginary parts, indicating a significant relative phase between them in these kinematics. Even though the underlying dynamics is quite different, the interference pattern obtained just above threshold for proton targets is quite similar to the corresponding shape determined from the data of Ref. [19] in the diffractive regime.

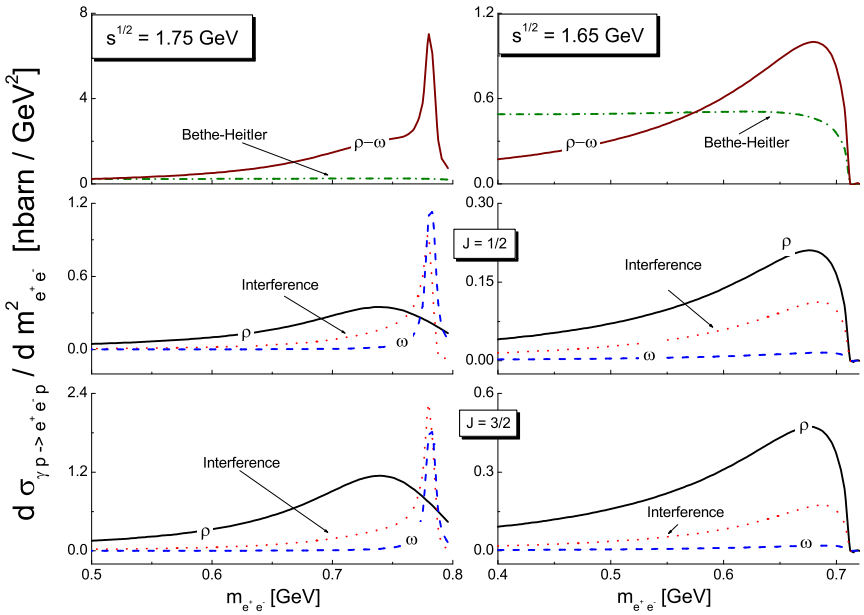

Fig. 4. Integrated spectra for the $\gamma p \to e^+e^-p$ reaction at $\sqrt{s}$=1.75 and 1.65 GeV together with their different components.

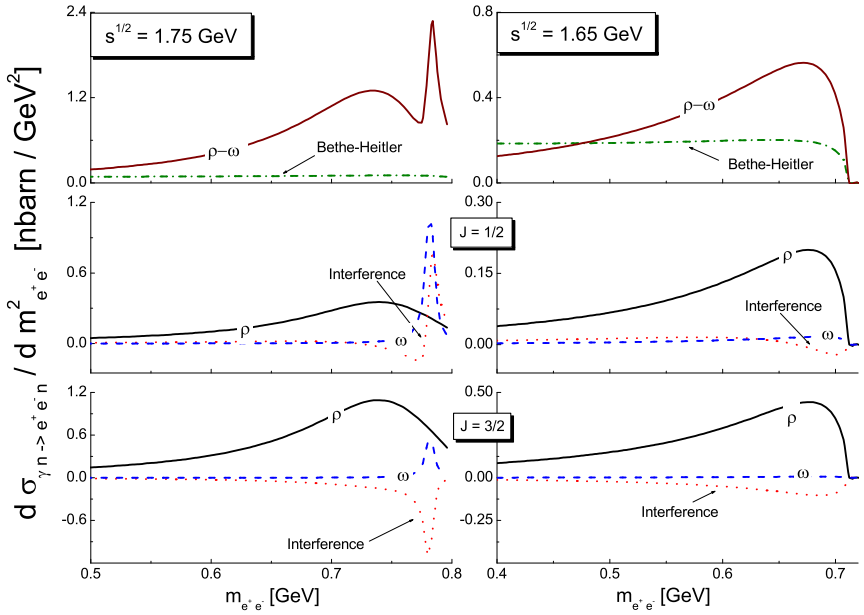

Fig. 5. Same as Fig. 4 for the $\gamma n \to e^+e^-n$ reaction.

Close but below threshold, at $\sqrt{s}$=1.65 GeV, the contributions of the Bethe-Heitler and vector meson production processes to the differential cross sections become comparable. All experimental studies of the vector meson photoproduction amplitudes below threshold in the dilepton channel will therefore require a careful subtraction of the Bethe-Heitler contribution. Below the ω-meson production threshold, the ρ-meson production and decay into e^+e^- pairs dominates the vector meson contribution. The $\gamma N \to e^+e^-N$ reaction is therefore a very useful tool to study ρ-meson photoproduction below threshold. In this regime the $\gamma N \to \rho N$ process is indeed very hard to extract from the $\gamma N \to \pi^+\pi^-N$ cross section because of the large contribution of the $\gamma N \to \Delta\pi$ reaction. We observe again that the $\rho - \omega$ interference is constructive for proton targets and destructive for neutron targets.

We display in Fig. 6 the integrated spectra for the $\gamma p \to e^+e^-p$ and $\gamma n \to e^+e^-n$ reactions at $\sqrt{s}$=1.55 GeV. This particular center of mass energy is of much interest because the amplitudes depend sensitively on the presence of two resonances whose coupling to vector mesons is poorly known, the $N^*_{3/2^-1/2}(1520)$ and the $N^*_{1/2^-1/2}(1535)$ (see Fig. 3). The Bethe-Heitler pairs are dominant for all pair invariant masses. The $\rho - \omega$ interference is large and intricate. It leads to particularly small cross sections for neutron targets.

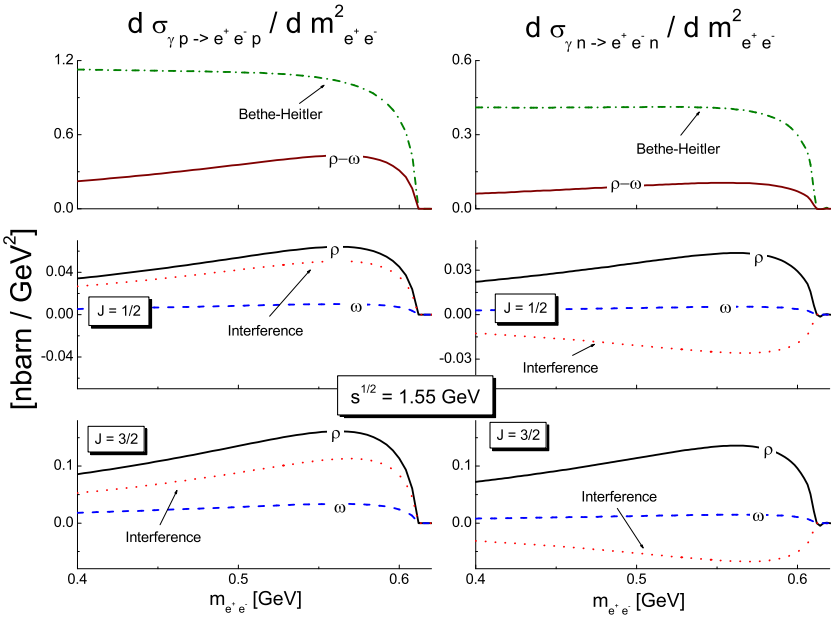

Fig. 6. Integrated spectra for the $\gamma p \to e^+e^-p$ and $\gamma n \to e^+e^-n$ reactions at $\sqrt{s}$=1.55 GeV together with their different components.

In Fig. 7 and 8, we show the $\sqrt{s}$ dependence of $\mathrm{d}\sigma/\mathrm{dm}^2_{e^+e^-}$ for given values of the e^+e^- pair invariant mass, $\mathrm{m}_{e^+e^-}$=0.55 GeV and 0.65 GeV. We recall that our model is valid for values of $\mathrm{m}_{e^+e^-}$ not too far from ($\sqrt{s}$ - M_N). It is nevertheless interesting to draw the cross sections over a large range of energies to see the relative behaviours of the Bethe-Heitler and vector meson cross sections, keeping the above restriction in mind.

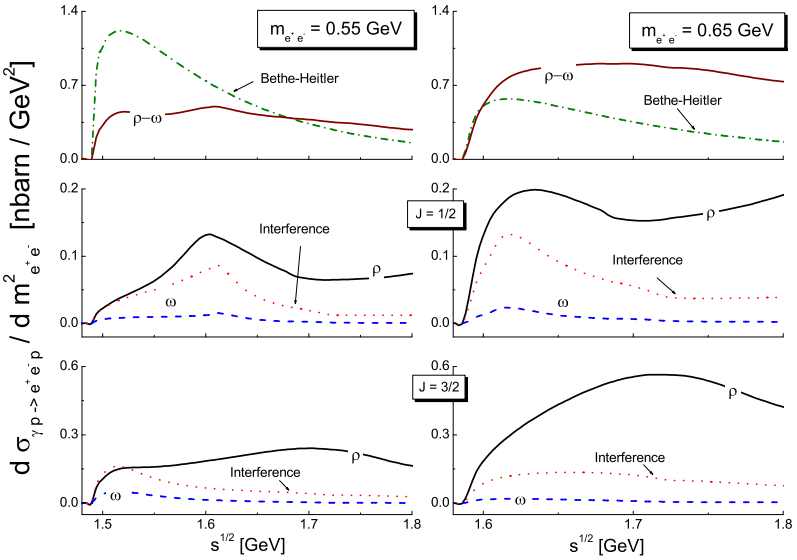

Fig. 7. Integrated spectra for the $\gamma p \to e^+e^-p$ reaction as function of $\sqrt{s}$ for two e^+e^- pair invariant masses.

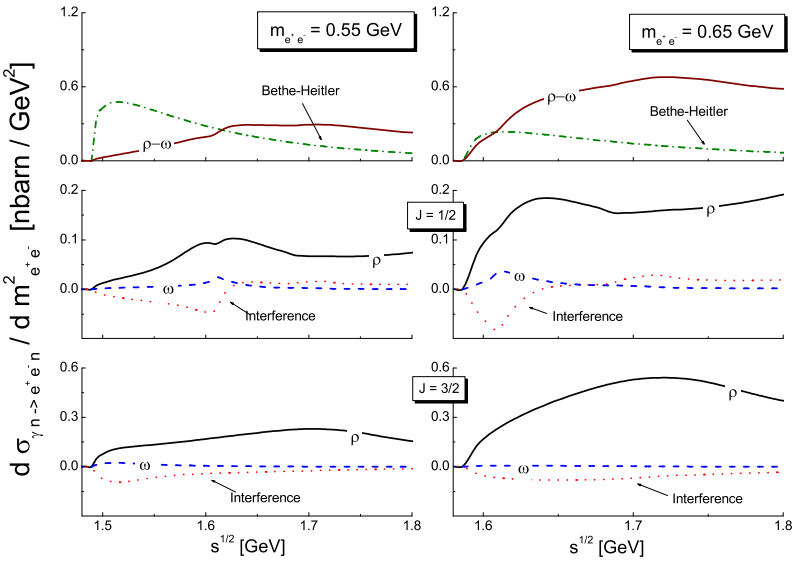

Fig. 8. Same as Fig. 7 for the $\gamma n \to e^+e^-n$ reaction.

We present now results for the symmetric and asymmetric cross sections defined by Eq. (24). We display them first integrated over the e^+e^- pair scattering angle in Figs. 9 and 10 at $\sqrt{s}$=1.75 and 1.65 GeV for the $\gamma\, p \to e^+e^-p$ and the $\gamma\, n \to e^+e^-n$ reactions respectively. The symmetric part is the total cross section and hence the sum of the Bethe-Heitler and vector meson cross sections shown in Figs. 4 and 5. The antisymmetric part reflects the interference of the Bethe-Heitler and vector meson pairs. The comparison of the symmetric and antisymmetric cross sections calls first for a general remark: the antisymmetric cross section is much smaller (by more than two orders of magnitude in the mass range of interest) than the symmetric cross section. The asymmetric cross section consists of terms reflecting the interference of Bethe-Heitler pairs with ρ-meson and ω-meson decay pairs respectively. We see from Figs. 9 and 10 that the Bethe-Heitler ρ-meson interference is the dominant contribution, except for pairs arising from the decay of ω-mesons produced on the mass-shell slightly above threshold.

To gain understanding of these results, we show in Figs. 11 and 12 the angular dependence of the Bethe-Heitler, vector meson and interference contributions. The angle θ is the emission angle of the e^+e^- pair in the center of mass frame. Figs. 11 and 12 indicate that the pairs originating from Bethe-Heitler processes and vector meson decays are produced in very different regions of phase-space. The Bethe-Heitler pairs are emitted at forward angles while e^+e^- pairs from vector meson decays are produced isotropically in the center of mass (recall that we consider only s-wave vector meson-nucleon channels). The Bethe-Heitler spectra peak strongly at low e^+e^- pair invariant masses, while vector meson decay is enhanced by the proximity of the poles for large e^+e^- pair masses. Consequently the quantum interference between the two processes is very small and most significant at small angles where the Bethe-Heitler cross section is very large.

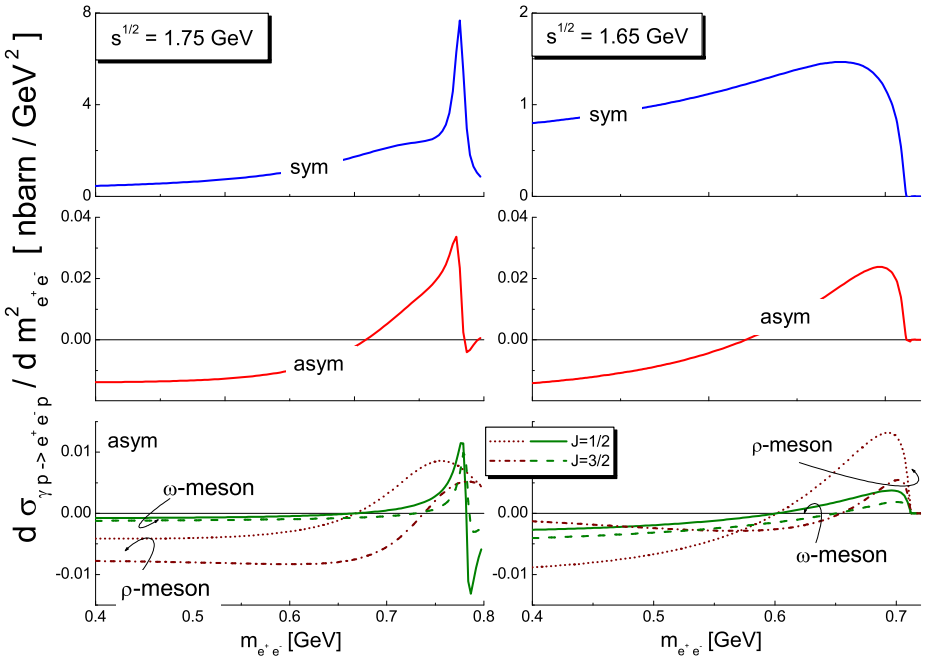

Fig. 9. Symmetric and asymmetric contributions to the $\gamma p \to e^+e^-p$ cross section at $\sqrt{s}$=1.75 and 1.65 GeV together with their different components.

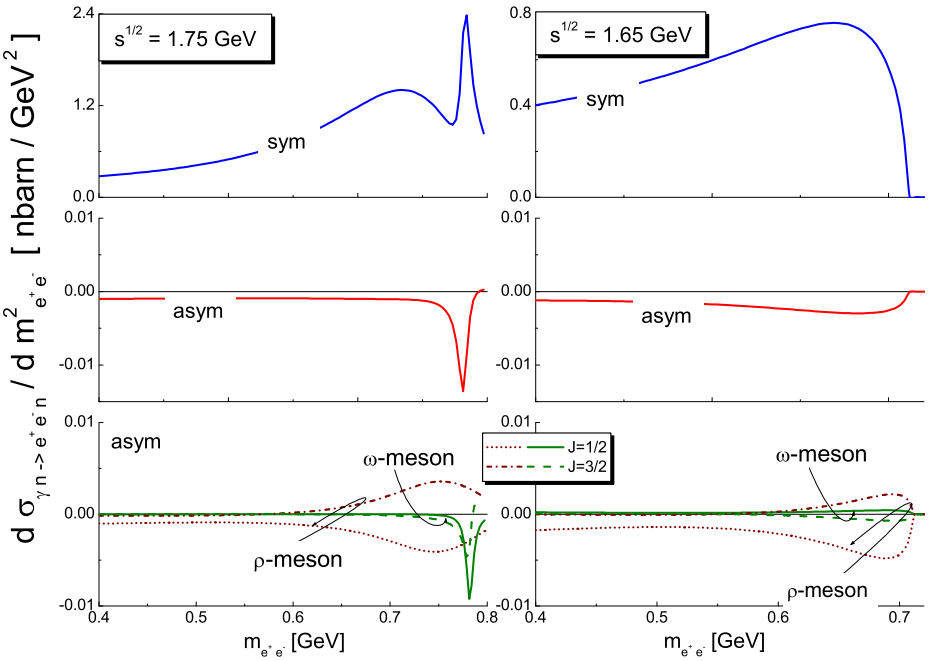

Fig. 10. Same as Fig. 9 for the $\gamma n \to e^+e^-n$ reaction.

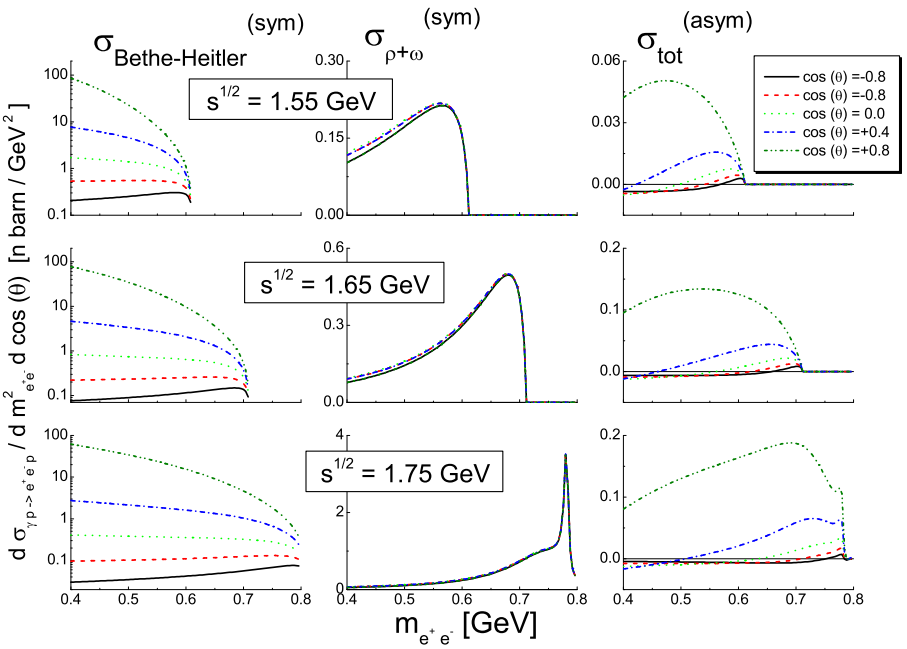

Fig. 11. Angular dependence of the Bethe-Heitler, vector meson and interference contributions to the $\gamma p \to e^+e^-p$ cross section at $\sqrt{s}$=1.75, 1.65 and 1.55 GeV. The angle θ is the emission angle of the e^+e^- pair in the center of mass frame.

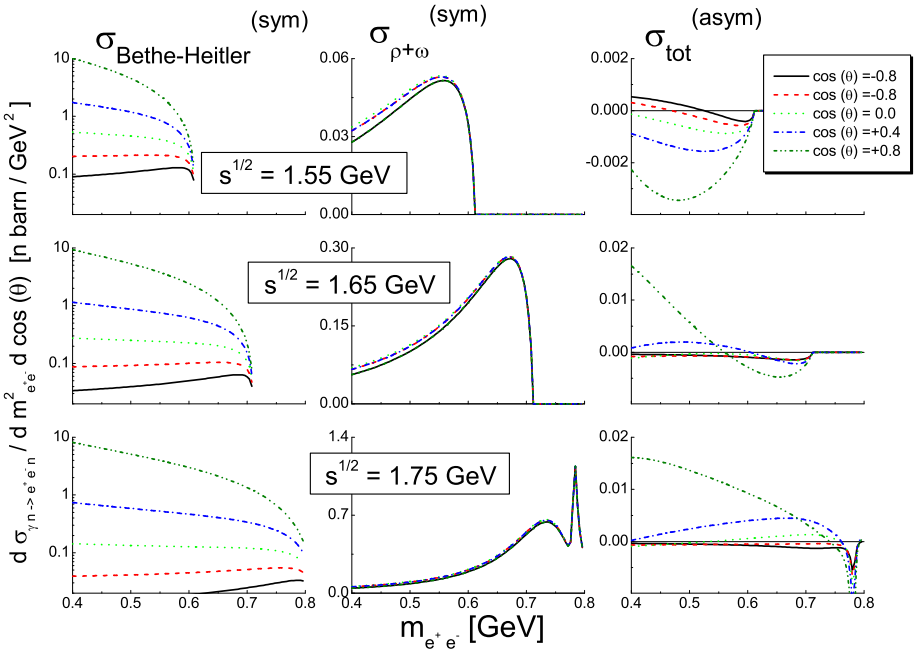

Fig. 12. Same as Fig. 11 for the $\gamma n \to e^+e^-n$ reaction.

5 Concluding remarks

We have studied the $\gamma p \to e^+e^-p$ and $\gamma n \to e^+e^-n$ cross sections close to the vector meson production threshold ($1.4 < \sqrt{s} < 1.8$ GeV). We have calculated the Bethe-Heitler and the vector meson decay contributions as well as their quantum interference. The Bethe-Heitler term is well-known and very accurately determined. The ρ- and ω-meson decay contributions are computed using the relativistic and unitary coupled-channel approach to meson-nucleon scattering of Ref. [7], supplemented with the Vector Dominance assumption (17) for the time-like photon in the final state. This calculation was performed in exactly the same theoretical framework as our earlier study of the $\pi N \to e^+e^-N$ reaction [9].

The $\gamma N \to e^+e^-N$ processes involve two kinds of quantum interferences, the Bethe-Heitler-vector meson and the ρ-ω interferences. We found the Bethe-Heitler-vector meson interference to be small because the two processes populate very different regions of phase space. The ρ-ω interferences are large. They are constructive for the $\gamma p \to e^+e^-p$ cross section and destructive for the $\gamma n \to e^+e^-n$ process.

Our work shows that the $\gamma p \to e^+e^-p$ and $\gamma n \to e^+e^-n$ reactions below the ω-meson threshold are very sensitive to the coupling of low-lying baryon resonances to the ρ-meson field. The $\gamma p \to e^+e^-p$ due to the e^+e^- decay of vector mesons in this regime can be determined from the total cross section, as the Bethe-Heitler term can be calculated and subtracted while its interference with vector meson pairs can be neglected. Data on the $\gamma p \to e^+e^-p$ process close and below threshold would be therefore most useful to provide constraints on the coupling of low-lying baryon resonances to the ρ-meson field. These couplings are difficult to determine from other reactions and play a major role in the dynamics of vector meson propagation in nuclear matter.

6 Acknowledgment

One of us (M.S.) is indebted to James J. Kelly for providing her with a very complete set of data on the nucleon electric and magnetic form factors. She acknowledges the hospitality of the GSI Theory Group where part of this work was done. We enjoyed discussing with Chaden Djalali about the experiment ongoing at JLab with the CLAS detector on the issues studied in this paper.

7 Appendix

In this appendix we provide some details on the derivation of the analytical results (27, 29, 30, 31, 32) displayed in Section 3. First we give an explicit definition for the coefficient $C_{\rm BH}$ characterizing the differential Bethe-Heitler cross section

$$
\begin{aligned}
&C_{\rm BH}(s,t,\bar{q}^2) = -m_e^2\, N^{\mu\nu}_{\rm BH}(\bar{p},p)\,\langle E^{\rm BH}_{\mu\nu}\rangle(\bar{q},q)\,,\\
&N^{\mu\nu}_{\rm BH}(\bar{p},\,p) = {\rm tr}\,\Big[\Big(|e|\,F_1^{(p)}(t)\,\gamma^\mu + \frac{i\,|e|}{2\,M_p}\,F_2^{(p)}(t)\,\sigma^{\mu\alpha}\;(\bar{p}-p)_\alpha\Big)\,\frac{\not{p}+M_p}{2\,M_p}\\
&\qquad\qquad\times\Big(|e|\,F_1^{(p)}(t)\,\gamma^\nu - \frac{i\,|e|}{2\,M_p}\,F_2^{(p)}(t)\,\sigma^{\nu\beta}\;(\bar{p}-p)_\beta\Big)\,\frac{\not{\bar{p}}+M_p}{2\,M_p}\Big]\,,\\
&E^{\mu\nu}_{\rm BH}(p_+,p_-,q) = {\rm tr}\,\Big[\frac{\not{p}_- + m_e}{2\,m_e}\,L^{\mu\alpha}(p_+,p_-,q)\,\frac{\not{p}_+ - m_e}{2\,m_e}\,\gamma_0\,L^{\dagger,\nu}{}_\alpha(p_+,p_-,q)\,\gamma_0\Big]\,,\\
&L_{\mu\nu}(p_+,p_-,q) = \gamma_\mu\,\frac{1}{\not{q}-\not{p}_+-m_e}\,\gamma_\nu + \gamma_\nu\,\frac{1}{\not{p}_- - \not{q} - m_e}\,\gamma_\mu\,,
\end{aligned}
\tag{33}
$$

where we introduced the phase-space average $\langle..\rangle$ of any Lorentz tensor $E_{\mu_1,\ldots,\mu_n}$

$$
\begin{aligned}
\langle E_{\mu_1\ldots\mu_n}\rangle(\bar{q},q) = \frac{\pi}{m_e^2}\,\sqrt{\frac{\bar{q}^2}{\bar{q}^2-m_e^2}}\int\frac{d^3\vec{p}_+}{(2\pi)^3}\,\frac{m_e}{p_+^0}\int\frac{d^3\vec{p}_-}{(2\pi)^3}\,\frac{m_e}{p_-^0}\\
\times\theta[q\cdot(p_+-p_-)]\,E_{\mu_1\ldots\mu_n}(p_+,p_-,q)\,(2\pi)^4\,\delta^4(\overline{q}-p_+-p_-).
\end{aligned}
\tag{34}
$$

The phase-space average is normalized by $\langle 1\rangle(\bar{q},q)=1$. In order to derive an analytic expression for $C_{\rm BH}(s,t,\bar{q}^2)$ it is advantageous to evaluate the phase-space average of the tensor $E^{\rm BH}_{\mu\nu}(p_+,p_-,q)$ as introduced in (34) first. In a second step we contract the result with the tensor $N^{\mu\nu}_{\rm BH}(\bar{p},p)$. The calculation is streamlined considerably by using the identity

$$
\langle E_{\mu\nu}\rangle(\bar{q},q) = \langle E_{\alpha\beta}\,T^{\alpha\beta}\rangle\,T_{\mu\nu}(\bar{q},q) + \sum_{i,j}\langle E_{\alpha\beta}\,L^{\alpha\beta}_{ij}\rangle\,L^{(ij)}_{\mu\nu}(\bar{q},q)\,,
\tag{35}
$$

where we introduced a set of orthogonal Lorentz tensors

$$
\begin{aligned}
&T_{\mu\nu}(\bar{q},q) = g_{\mu\nu} - \frac{\bar{q}_\mu\,\bar{q}_\nu}{\bar{q}^2} - X_\mu\,X_\nu\,,\qquad X_\mu = i\,\frac{q_\mu\,\bar{q}^2 - \bar{q}_\mu\,(\bar{q}\cdot q)}{\sqrt{\bar{q}^2}\,(\bar{q}\cdot q)}\,,\\
&L^{\mu\nu}_{11}(\bar{q},q) = \frac{\bar{q}_\mu\,\bar{q}_\mu}{\bar{q}^2}\,,\qquad L^{\mu\nu}_{22}(\bar{q},q) = X^\mu\,X^\nu\,,\\
&L^{\mu\nu}_{12}(\bar{q},q) = \frac{\bar{q}^\mu}{\sqrt{\bar{q}^2}}\,X_\nu\,,\qquad L^{\mu\nu}_{21}(\bar{q},q) = X_\mu\,\frac{\bar{q}^\mu}{\sqrt{\bar{q}^2}}\,.
\end{aligned}
\tag{36}
$$

By means of (35,36) the evaluation of the Bethe-Heitler differential cross section (24, 27) reduces to straightforward, though somewhat tedious algebra. The phase-space average can be performed in the center-of-mass frame of the lepton pair. The only integration to be performed anew is the one over the angle defined by the incoming photon and outgoing lepton three-momenta, i.e. $0 < \cos(\vec{q}, \vec{p}_-) < 1$. This follows since all other scalar products of the available 4-momenta, $\bar{q}, \bar{p}, q$, and p are determined uniquely by $s, t, \bar{q}^2$ and the mass parameters.

The computation of the functions $C_{\rm VM}^{(JJ',h)}$, characterizing the contributions of the photo-induced vector meson production amplitudes, is analogous once we have introduced the definition

$$
\begin{aligned}
&\sum_h C_{\rm VM}^{(JJ',h)}(s,t,\bar{q}^2)\,\sqrt{N_{Jh}^{(V)}}\,\sqrt{N_{J'h}^{(V')}} = -m_e^2\,N^{\mu\nu}_{JV,J'V'}(\bar{p},p)\,\langle E^{\rm VM}_{\mu\nu}\rangle(\bar{q},q)\,,\\
&N^{\alpha\beta}_{JV,J'V'} = {\rm tr}\,\Big[\frac{\not{p}+M_p}{2\,M_p}\;P^{(J)}_{\alpha\nu}(w)\,\Gamma^{\nu}_{V,\,\mu}(q,w)\\
&\qquad\qquad \times\frac{\not{p}+M_p}{2\,M_p}\,\gamma_0\,\Gamma^{\dagger\bar{\nu}}_{V',\,\mu}(q,w)\,P^{(\dagger J')}_{\beta\bar{\nu}}(w)\,\gamma_0\Big]\,,\\
&E^{\mu\nu}_{\rm VM} = {\rm tr}\,\Big[\frac{\not{p}_-+m_e}{2\,m_e}\,\gamma^\mu\,\frac{\not{p}_+-m_e}{2\,m_e}\,\gamma^\nu\Big]\,,
\end{aligned}
\tag{37}
$$

where the normalization factors are given in Eq. (16). The factorization of the normalization factors implied by the (l.h.s) of (37) is not obvious but can be shown by an explicit calculation. This formulation leads, after some algebra, to the analytic expressions (29).

Most tedious is the derivation of the expressions (30-32), characterizing the interference of the Bethe-Heitler pairs with those produced by the decay of the vector mesons. We write

$$
\begin{aligned}
&\sum_h C_{\rm asym}^{(Jh)}\,\sqrt{N_{Jh}^{(V)}} = -m_e^2\,N_{VJ}^{\alpha\beta,\mu}\,\langle E^{\rm asym}_{\alpha\beta,\mu}\rangle\,,\\
&E^{\alpha\beta,\mu}_{\rm asym} = {\rm tr}\,\Big[\frac{\not{p}_-+m_e}{2\,m_e}\,\gamma^\alpha\,\frac{\not{p}_+-m_e}{2\,m_e}\,\gamma_0\,L^{\dagger,\beta}{}_{\mu}(p_+,p_-,q)\,\gamma_0\Big]\,,\\
&N_{VJ}^{\alpha\beta,\mu} = {\rm tr}\,\Big[\frac{\not{p}+M_p}{2\,M_p}\,\Big(|e|\,F_1^{(p)}(t)\,\gamma^\beta + \frac{i\,|e|}{2\,M_p}\,F_2^{(p)}(t)\,\sigma^{\beta\bar{\beta}}\,(\bar{p}-p)_{\bar{\beta}}\Big)\\
&\qquad\qquad \times\frac{\not{p}+M_p}{2\,M_p}\,\gamma_0\,\Gamma^{\dagger\bar{\nu}}_{V,\,\mu}(q,w)\,P^{(\dagger J)}_{\alpha\bar{\nu}}(w)\,\gamma_0\Big]\,,
\end{aligned}
\tag{38}
$$

where the consistency of the definition (38) can again be checked by an explicit calculation. The evaluation of the phase-space average in (38) is performed using a generalization of (35). The results are the coefficients (30-32).

References

[1] J.J. Sakurai, Currents and Mesons, The University of Chicago Press, 1969.

[2] N.M. Kroll, T.D. Lee and B. Zumino, Phys. Rev. 157 (1967) 1376.

[3] A.I. L'vov, V.A. Petrun'kin, M. Schumacher, Phys. Rev. C 55 (1997) 359.

[4] G. Laveissière et al., hep-ex/0406062.

[5] G. Laveissière et al., Phys. Rev. C 69 (2004) 045203.

[6] D.O. Riska and G.E. Brown, Nucl. Phys. A 679 (2001) 577.

[7] M.F.M. Lutz, Gy. Wolf and B. Friman, Nucl. Phys. A 706 (2002) 431.

[8] S. Capstick and W. Roberts, Prog. Part. Nucl. Phys. 45 (2000) S241.

[9] M.F.M. Lutz, B. Friman, M. Soyeur, Nucl. Phys. A 713 (2003) 97.

[10] J.G. Messchendorp, Nucl. Phys. A 684 (2001) 493_c.

[11] D. Trnka, Diplomarbeit, II. Physikalisches Institut der Justus-Liebig-Universität Giessen, April 2002.

[12] JLab/Hall B/E-01-112 Proposal.

[13] J.J. Kelly, Phys. Rev. C 66 (2002) 065203.

[14] S.D. Drell and J.D. Walecka, Ann. Phys. 28 (1964) 18.

[15] M.F.M. Lutz and E.E. Kolomeitsev, Nucl. Phys. A 700 (2002) 193.

[16] B. Friman and M. Soyeur, Nucl. Phys. A 600 (1996) 477.

[17] W.H. Furry, Phys. Rev. 51 (1937) 125.

[18] A. Yu. Korchin, O. Scholten, Phys. Rev. C62 (2000) 015205.

[19] H. Alvensleben et al., Nucl. Phys. B 25 (1971) 333.

[20] A. Yu. Korchin, O. Scholten, F. de Jong, Phys. Lett. B 402 (1997) 1.

[21] A. I. L'vov et al., Phys. Rev. C 57 (1998) 312.

[22] H. Alvensleben et al., Nucl. Phys. B 25 (1971) 342.